Experiments on animals and animal tissues

It is a requirement of the Society that all vertebrates (and Octopus vulgaris) used in experiments are humanely treated and, where relevant, humanely killed.

To this end authors must tick the appropriate box to confirm that:

For work conducted in the UK, all procedures accorded with current UK legislation.

For work conducted elsewhere, all procedures accorded with current national legislation/guidelines or, in their absence, with current local guidelines.

Experiments on humans or human tissue

Authors must tick the appropriate box to confirm that:

All procedures accorded with the ethical standards of the relevant national, institutional or other body responsible for human research and experimentation, and with the principles of the World Medical Association's Declaration of Helsinki.

Guidelines on the Submission and Presentation of Abstracts

Please note, to constitute an acceptable abstract, the Society requires the following ethical criteria to be met. To be acceptable for publication, experiments on living vertebrates and Octopus vulgaris must conform with the ethical requirements of The Society regarding relevant authorisation, as indicated in Step 2 of submission.

Abstracts of Communications or Demonstrations must state the type of animal used (common name or genus, including man. Where applicable, abstracts must specify the anaesthetics used, and their doses and route of administration, for all experimental procedures (including preparative surgery, e.g. ovariectomy, decerebration, etc.).

For experiments involving neuromuscular blockade, the abstract must give the type and dose, plus the methods used to monitor the adequacy of anaesthesia during blockade (or refer to a paper with these details). For the preparation of isolated tissues, including primary cultures and brain slices, the method of killing (e.g. terminal anaesthesia) is required only if scientifically relevant. In experiments where genes are expressed in Xenopus oocytes, full details of the oocyte collection are not necessary. All procedures on human subjects or human tissue must accord with the ethical requirements of the Society regarding relevant authorisation, as indicated in Step 2 of submission; authors must tick the appropriate box to indicate compliance.

PL04

Structural synaptic plasticity during long-term potentiation (LTP)

Kristen Harris[1]

[1]University of Texas at Austin, United States

Synapses form trillions of connections in the brain. Long-term potentiation (LTP) is a cellular mechanism vital for learning that modifies the strength and structure of synapses. Three-dimensional electron microscopy reveals distinct pre- to post-synaptic arrangements. Strong active zones have tightly docked presynaptic vesicles, weak active zones have loose or non-docked vesicles, and nascent zones have a postsynaptic density but no presynaptic vesicles. LTP can be temporarily saturated, which prevents further increases in synaptic strength. We have used 3D reconstruction from serial section electron microscopy to discover how the plasticity of nascent zones provides a time dependent and synapse-specific expansion of active zones during LTP. This expansion ultimately encourages the formation of highly effective dendritic spine clusters regulated by the spine apparatus. I will introduce our rat model system with knockout of synaptopodin as a basis for investigating the cluster hypothesis. We hypothesize that the saturation of LTP protects recently formed memories and that regrowth of nascent zones accounts for the advantage of spaced over massed learning.

SA01

Synaptic signaling in the human hippocampal CA3 network

Peter Jonas[1]

[1]Institute of Science and Technology Austria (ISTA), Austria

The hippocampal CA3 network is the largest autoassociative network in the mammalian brain. CA3 pyramidal neurons are connected to each other through recurrent synapses endowed with Hebbian synaptic plasticity, forming an almost infinitely large synaptic matrix for storage and retrieval of information. In humans, the number of CA3 pyramidal neurons is 1.7 million, more than an order of magnitude higher than in mice (110,000). How this huge difference in cell numbers impacts on synaptic function and connectivity remains unclear.

To address this question, we applied cutting-edge electrophysiology and superresolution-expansion microscopy to slices from the human hippocampus. Recordings were focused on tissue from MRI-negative patients ("nonsclerotic"), in which cellular organization was largely preserved. Neuronal density in the CA3 region in MRI-negative patients was similar to that of postmortem tissue, further suggesting that the circuit may approach the physiological situation. We first characterized the CA3 network by multicellular patch clamp-based circuit mapping, and found that the recurrent CA3–CA3 synapse was characterized by high reliability and sparse connectivity. The average connectivity was 1.27%, substantially lower than in mice. To investigate the determinants of connectivity, we analyzed the number of spines in CA3 pyramidal neurons dedicated to the recurrent collateral inputs using superresolution-expansion microscopy. In humans, CA3 pyramidal cells had 16,100 spines, only moderately higher than in mice (13,200). Thus, our results indicate that cell number is the main determinant of connectivity, and suggest an inverse scaling rule between connectivity and cell number across species.

We next characterized the mossy fiber input by paired recordings between mossy fiber terminals and CA3 pyramidal neurons. Presynaptic mossy fiber terminals were stimulated in the non-invasive bouton-attached configuration. We found that stimulation of single stimuli in presynaptic terminals reliably triggered spiking in postsynaptic CA3 pyramidal neurons, demonstrating that the human mossy fiber synapse acts as a "detonator". To assess connectivity, we estimated the number of large terminals impinging on the apical dendrites of CA3 pyramidal neurons using superresolution-expansion microscopy. In humans, single CA3 pyramidal neurons received inputs from 280 mossy fiber terminals, ~fivefold more than in mice (~50). Although the number of inputs per cell is higher, the total granule cell-to-CA3 pyramidal neuron connectivity is lower in humans. While the higher number of mossy fiber inputs per cell may enhance combinatorial coding, the sparse connectivity may facilitate pattern separation.

Taken together, our results show that both CA3–CA3 recurrent collateral synapses and mossy fiber synapses on CA3 pyramidal neurons follow complex evolutionary scaling rules, which may enhance the computational power of the human brain.

SA02

Nanostructural regulation of synaptic transmission

Thomas Blanpied[1]

[1]University of Maryland School of Medicine, US

Dissecting the mechanisms of synaptic transmission touches on nearly all fields of neuroscience. Work over recent years has made clear that protein distribution within single synapses is highly organized across multiple spatial scales ranging from the nanoscale accumulation of just a few protein molecules to larger domains with unique multiprotein compositions. I will address recent data regarding synaptic molecular organization to argue that the complexity of synaptic nanostructure generates functional capabilities that can fine-tune synaptic strength and augment the capabilities of classical quantal synaptic transmission. PSD-95 serves a case study for how to approach the emergent problem of describing and classifying forms of protein organization, including trans-synaptic “nanocolumn” relationships between AMPA receptors and glutamate release sites. Recent work identifying features of NMDA receptor subsynaptic organization suggests that these patterns also are likely to regulate the patterns of neural activity which can induce synaptic plasticity. The capacity of next-generation light microscopy to measure within synapses at sub-molecular resolution offers new routes to understanding the link between biochemical mechanisms and synapse physiology.

SA03

Location-dependent cholinergic biased signalling regulates axonal intrinsic plasticity in hippocampal neurons

Haojie Sun[1], Rafael Lujan[2], Xuewei Yu[1], Ryan Dowsell[3], Timothy Church[1], Katharine Gibson[4], Andrew Tobin[4], Matthew Gold[1], Mala Shah[1]

[1]University College London, UK, [2]Universidad Castilla La Mancha, Spain, [3]University College London , UK, [4]University of Glasgow, UK

Acetylcholine is a neuromodulator that critically regulates cognition by activating muscarinic M1 receptors. Interestingly M1 receptors are located throughout neurons (including at the axon initial segment (AIS)). Activation of these have a variety of location-dependent effects on neuronal activity. We have explored the intracellular mechanisms underpinning these diverse location-dependent effects. We find that stimulation of M1 receptors at the AIS triggers beta-arrestin 2 and not G-proteins to induce a persistent reduction in the action potential threshold and enhanced neuronal firing. This intrinsic plasticity was dependent on agonist-induced phosphorylation of M1 receptors by casein kinase 2. Beta-arrestin 2 recruitment by M1 receptors initiated a unique downstream signalling pathway. In contrast, soma-dendrite M1 receptor activation instigated G-protein signalling to reversibly modify membrane properties. Our findings reveal that M1 receptors situated in distinct compartments diversely transform hippocampal neuron activity by triggering unique signalling modalities – a process we term location-dependent system bias.

C01

Presynaptic ultrastructure and vesicle mobility at cerebellar and hippocampal mossy fibre boutons support their functional divergence

Jason Rothman[1], Noemi Holderith[2], Carolina Borges-Merjane[3], William Pryke[4], Peter Jonas[5], Angus Silver[4]

[1]Department of Neuroscience, Physiology and Pharmacology, University College London, UK, [2]Laboratory of Cellular Neurophysiology, Institute of Experimental Medicine, Hungary, [3]Biozentrum of the University of Basel, Basel, [4]Department of Neuroscience, Physiology and Pharmacology, University College London, United Kingdom, [5]Cellular Neuroscience, Institute of Science and Technology Austria, Austria

Introduction. *In vivo*, cerebellar mossy fibre boutons (cMFBs) can sustain high-frequency transmission which is well-suited for rate coded signalling, while hippocampal mossy fibre boutons (hMFBs) exhibit strong facilitation which is well-suited for burst coding. Despite sharing a common name and gross morphological features, it is unclear whether differences in presynaptic ultrastructure contributes to their distinct functional properties.

Aims. We compared the presynaptic ultrastructure and vesicle mobility in cMFBs and hMFBs to determine whether they contribute to the different vesicle supply rates required for sustained rate and burst signalling in these axons.

Methods. Boutons from wild type mouse cerebellar and hippocampal tissue were analysed by transmission electron microscopy and electron tomography. Mitochondrial size and area fraction, active zone (AZ) surface area, and vesicle size and density were quantified stereologically [1]. Vesicle mobility was measured in acute slices from VGLUT1-Venus mice using fluorescence recovery after photobleaching (FRAP; 35°C) [2]. Biologically constrained 3D Monte Carlo simulations were used to model FRAP data and to predict sustained vesicle supply to multiple AZs.

Results. Mitochondria in cMFBs were larger (short-axis diameter: 243.8 ± 5.7 nm, n = 36 images) than in hMFBs (191.2 ± 3.0 nm, n = 26; $p < 0.001$, t-test) and more densely packed (area fraction: 0.224 ± 0.012 vs 0.076 ± 0.005; $p < 0.001$). AZs were significantly smaller in cMFBs (0.040 ± 0.006 μm^2, n = 8 AZs) than hMFBs (0.110 ± 0.026 μm^2, n = 8, p = 0.03, t-test), with lower docked vesicle density (102.4 ± 8.0, n = 20 vs 160.3 ± 10.6 vesicles/μm^2, n = 20, $p < 0.001$). Vesicle diameters were larger (45.4 ± 0.5 nm, n = 41 VOIs vs 44.0 ± 0.2 nm, n = 31, p = 0.007, t-test) and more variable in cMFBs, while vesicle cluster volume fraction was lower (0.340 ± 0.015 vs 0.418 ± 0.007; $p < 0.001$, t-test). FRAP revealed a 9-fold slower long-time diffusion coefficient in hMFBs (Dlong = 2.7 ± 1.1 × 10^{-3} μm^2/s, n = 79 boutons) compared to cMFBs (24.5 ± 3.6 × 10^{-3} μm^2/s, n = 63; $p < 0.001$, model F-test), with 2-fold smaller mobile fraction (40 ± 6% vs 76 ± 1%; $p < 0.001$). Monte Carlo simulations predicted that the higher vesicle density and larger immobile fraction can fully account for the reduced mobility in hMFBs. Simulations of vesicle supply to multiple AZs predicted that the smaller, spatially distributed AZs of cMFBs can support sustained vesicle delivery longer than the larger AZs of hMFBs.

Conclusions. Our results show that cMFBs and hMFBs differ substantially in mitochondrial content, AZ size, vesicle packing and mobility. These ultrastructural differences, and 9-fold difference in vesicle mobility, contribute to their distinct functional properties, supporting higher energy and vesicle supply requirements for sustained rate coding at cerebellar synapses and approximately 4-fold larger pool of docked vesicles required for burst coding at hippocampal synapses.

Ethics. Procedures were carried out in accordance with the UK Animals (Scientific Procedures) Act 1986, approved by relevant institutional ethics committees.

C02

Physiological constraints and ultrasonic hearing in the mammalian cochlea

Jonathan Ashmore[1]

[1]University College London, UK

In young humans, the upper limit of the hearing range is approximately 18 kHz, but in most mammals the range can extend to 100 kHz. The basic physiological tuning mechanism depends on how sound propagates in the fluid of the cochlear duct: it excites a place specific vibration of the basilar membrane (BM) that is enhanced by a population of sensory hair cells, outer hair cells (OHCs). These cells exhibit what is termed 'electromotility'. Subsequently inner hair cells (IHCs) signal tonotopic information to the brain. Although qualitatively simple, quantitative descriptions are complex and multiscale because 1) the OHC mechano-transduction step is non-linear; 2) there may be intrinsic bandwidth limits to the sensory process either from filtering by the membrane times constant or from inherent limits of the underlying molecular 'motor (prestin/SLC26A5) and 3) there is limited access to all points along the cochlea and consequent sparse data, although now improving with better imaging technologies.

The approach here is to show that some of these issues can be overcome using a model that incorporates realistic cochlear geometry (Geisler, 1993) and using parameters from a variety of sources. The essential model features include 1) the OHC length which depends, independent of species, on their characteristic frequency; 2) the orientation of the tectorial membrane (TM) which is angled more steeply to the BM as the characteristic frequency increases; 3) a 'piezo-electric' property (reverse electromotility) of OHCs, whereby longitudinal force on the cells generates current that compensates for the membrane time constant; 4) an intrinsic time constant (ca 16 us) of relaxation of the prestin/SLC26A5 driving OHC electromotility (Gale & Ashmore, 1997). A Green's function approach is used to incorporate the effects of fluid coupling between adjacent sections. Reasonable cochlear frequency tuning curves, agreeing with experimental data, can be obtained for both low and high frequencies up to 70 kHz. Age-related human hearing loss may depend on some of these mechanism being compromised.

All computations are performed in a linear approximation appropriate for threshold measurement. A graphic interface written in Matlab will be available on request.

C03

Four phases and a temporal threshold of population calcium response in cortical astrocytes during locomotion.

Anna Fedotova, Alexey Brazhe, Alexey Semyanov[1]

[1]Jiaxing University, China

Calcium activity is a major form of astrocyte excitability essential to their function and plasticity. Astrocytic calcium events arise both spontaneously and in response to behaviour. In this study, we examined how these unitary events shape population-level calcium activity during quiescence and locomotion. Using two-photon imaging of astrocytic calcium in the primary somatosensory cortex (S1) of awake mice running on a freely rotating disk, we found that spontaneous fluctuations during quiescence were driven mainly by the co-occurrence of new calcium events rather than by their enlargement. During locomotion, population responses progressed through four phases: the emergence of new events, their merging into a superevent, fragmentation of this superevent, and an afterburst. New events appeared immediately at locomotion onset, indicating a rapid astrocytic response. The response also exhibited a temporal threshold of ~5 seconds: when locomotion was shorter than this, the superevent phase failed to develop, and the population response was markedly reduced. In suprathreshold responses, the superevent displayed a ΔF/F intensity pattern that reproduced reliably across locomotion episodes. Hotspots within this pattern had shorter latencies and were also more active during quiescence, suggesting that the response is at least partly deterministic. Together, these findings dissect the population calcium response into quantifiable properties of unitary calcium events and reveal the formation and reproducibility of the superevent pattern.

C04

The Rhythm of Drinking: two hierarchically organized signals govern swallow timing in mice

Alastair MacDonald[1], Wen-Chun Lee[1], Kevin Yackle[1]

[1]University of California San Francisco, United States of America

Introduction: Swallowing is an essential step of ingestion that requires the passage of food or drink from the mouth into the gastrointestinal tract. This occurs in the pharynx, a multi-functional space that serves as the entrance to both the digestive and respiratory systems. Given the dual-purpose of the pharynx, swallowing must be correctly timed with concurrent digestive (oral transport) and respiratory (breathing) behaviours to avoid injury, aspiration or choking. Despite this complexity, swallowing occurs seamlessly while eating or drinking in most people. Since it is unknown how these rhythms are organized in drinking mammals and whether sensory input can modulate this organization, we investigated this in mice.

Methods: C57BL6/J mice (n= 8, 5M/3F) were implanted with a stainless-steel head bar to permit head-fixation. Following recovery, mice were restricted to drinking 1 ml of water per day to induce thirst. On test days, this water was delivered on a behavioural apparatus consisting of a lick spout connected to a solenoid-gated fluid delivery system and an external airflow sensor. The experiment consisted of mice licking from the spout, which triggered the solenoid to open and dispense 0.5 µl of water, followed by a short timeout period (200 ms) during which subsequent licks would not open the valve. By measuring solenoid opens and systematically varying the timeout (100-500 ms) we could control the rate of fluid delivery to the mouse and calculate the swallowed volume and the inter-swallow interval.

Results: We identified swallowing as brief (~50 ms) pauses in breathing. These events were nested in the ongoing breathing and licking rhythms, occurring at the phase transition from inhalation to exhalation in breathing and during the tongue retraction phase of licking. This phase-dependency meant that, immediately before a swallow, there was co-incident inhalation and tongue protrusion. We found that when mice were drinking, swallowing occurred at regular intervals. To test whether this was modulated by sensory input, we used a dynamic timeout protocol where the length of time between drops (and therefore the flow rate of the liquid) systematically decreased in 100 ms increments. We found that as the timeout decreased, the inter-swallow interval decreased accordingly. This resulted in a swallow volume ~4 µl across all timeouts.

Conclusion: By monitoring licking, breathing and swallowing during drinking in mice, we discovered two criteria that predict a swallow. First, that the breathing and licking rhythms must be aligned at a specific phase to permit swallowing. Second, swallowing will only occur after a certain volume of fluid has been accumulated and that delaying this rate of accumulation will delay the swallow. Furthermore, these two conditions are organized hierarchically, meaning that aligned breathing and licking only results in a swallow when the volume threshold has been met. This study has unmasked fundamental principles that determine swallow timing in mice and provides an experimental platform for the study of the sensory and circuit mechanisms that generate this behaviour.

Ethics statement: All experiments were performed in accordance with national and Institutional Animal Care and Use Committee guidelines.

C05

The Neonatal Brain at Birth: Region-Specific Neuronal Loss and Parallel Innate Immune Responses Following Intrauterine Escherichia coli K1 Infection

Romy Weinstock[1], Débora Magalhães Portela[2], Raissa Rilo Christoff[2], Alessio Delogu[3], Richard Wingate[4], Ashley Boyle[5], Patricia Pestana Garcez[4]

[1]Department of Neuroimaging, IoPPN, King's College London, UK, [2]Institute of Biomedical Sciences, Federal University of Rio de Janeiro, Brazil, [3]Department of Basic and Clinical Neuroscience, IoPPN, King's College London, UK, [4]Centre for Neurodevelopmental Disorders, IoPPN, King's College London, UK, [5]Department of Women and Children's Health, King's College London, Institute for Women's Health, UCL,, UK

Introduction

Escherichia coli K1 is a leading cause of neonatal bacterial meningitis, carrying 10-15% mortality and leaving 30-50% of survivors with lasting neurological damage. The mechanisms underlying this neuropathology remain poorly understood, particularly the innate immune responses involving resident microglia and peripheral immune infiltration.

Aims

This study aimed to characterise neonatal brains after intrauterine *E. coli* K1 infection, quantifying neuronal and microglial populations as primary outcomes, with exploratory analysis of mast cell infiltration and cerebellar external granule layer (EGL) thickness.

Methods

Fixed P0 brain tissue was obtained directly from the Boyle et al. (2025) cohort (E. coli K1-infected and PBS control C57BL/6 Tyrc-2J mice; n = 3-4 per group), a timepoint not previously examined in that study. All procedures were conducted under UK Home Office Licence PAD4E6357 in accordance with the Animals (Scientific Procedures) Act 1986. Sections were cut at 70 µm using a Leica vibratome. Immunofluorescence was performed for TUJ1 (neurons), IBA1 (microglia), and tryptase (mast cells), imaged on a Zeiss LSM880 confocal microscope. Cerebellar sections were stained with cresyl violet (Nissl) and imaged on a brightfield microscope. Neuronal and mast cell density were quantified by manual counting in ImageJ; microglial density and morphology were assessed by quantification and Sholl analysis. EGL thickness was measured in Fiji. Group differences were assessed using Welch's t-tests with the individual brain as the statistical unit.

Results

TUJ1-positive neuronal density was reduced by approximately 60% in infected animals (control: 203 ± 11; infected: 81 ± 6 cells per ROI; n = 3 per group; p = 0.0026). IBA1-positive microglial density was significantly elevated across all three cortical regions examined: lower cortical layer (p = 0.0223), upper cortical layer (p = 0.0402), and cortical white matter (p = 0.0453; n = 3 per group). A trend towards reduced process complexity in infected microglia was observed by Sholl analysis (p = 0.0525; n = 4 per group), consistent with a shift towards an activated morphology. Tryptase-positive mast cell density was approximately 5-fold higher in infected animals (control: 4.67 ± 1.45; infected: 23.67 ± 1.76 cells per

section; n = 3 per group; p = 0.0013). Cerebellar EGL thickness was reduced by 34% in infected animals (n = 4 per group; p = 0.0054).

Conclusions

E. coli K1 infection drives significant neuronal loss and concurrent activation of both resident (microglia) and peripheral (mast cell) innate immune populations at birth, alongside disruption of cerebellar development. These findings suggest neuropathology is established at birth and identify mast cell infiltration and cerebellar disruption as novel features of this model. Limitations include small sample sizes (n = 3-4) and a single timepoint. Future work should examine longitudinal trajectories and mast cell-microglia interactions as potential therapeutic targets.

C06

A Perineurial Cell-Mediated Leptin-Sympathetic Axis Protects against Obesity

Gitalee Sarker[1], Anandhakumar Chandran[2], Cyrielle Maroteau[2], Sofia Lundh[3], Karin Ziegler[4], Miguel Lopez Perez[5], Matteo Iannacone[6], Philipp E. Scherer[7], Enrique M. Toledo[2], Ana Domingos[8]

[1]University of Oxford, United Kingdom, [2]Research and Development, Novo Nordisk Research Centre Oxford, Oxford, United Kingdom, [3]Department of Pathology and Imaging, Global Drug Discovery, Novo Nordisk A/S, Måløv , Denmark, [4]Institute of Pharmacology and Toxicology, Technical University Munich (TUM), Munich, Germany, [5]CiMUS, Universidade de Santiago de Compostela, Santiago, Spain, [6]Vita-Salute San Raffaele University, Milan, Italy, [7]Touchstone Diabetes Center, The University of Texas Southwestern Medical Center, Dallas, USA, [8]Department of Physiology, Anatomy and Genetics, University of Oxford, United Kingdom

Introduction:

Obesity is a chronic, multifactorial disease typically associated with hyperleptinemia and leptin resistance, whereby leptin fails to promote its anticipated effects[1]. Efforts to better understand and define leptin resistance have largely focused on dissecting the mechanisms behind central leptin resistance. Recent studies show that leptin activates the sympathetic neurons innervating adipose tissue, promoting lipolysis[2] and thermogenesis[3] via neuronally released norepinephrine. Hence, the restoration of leptin sensitivity in adipose tissue could be a therapeutic target for obesity. However, the cellular and molecular players coordinating leptin and sympathetic signalling in adipose tissue remain poorly understood.

Aims/Objectives:

This study aims to identify and characterise cellular mediators coordinating leptin and sympathetic signalling in adipose tissue, and to determine their role in energy homeostasis and obesity.

Methods:

Single-cell RNA sequencing was performed on murine sympathetic ganglia (n = 20 mice) to identify novel cell populations. Conditional knockout mice targeting *Adrb2* in *Lepr*$^{+}$ cells (*Adrb2*KO) were generated for loss-of-function studies, with littermate controls (*Lepr*^{Cre} and *Adrb2*$^{fl/fl}$).

Metabolic phenotyping included body weight and food intake (n = 15-20 per group), energy expenditure (n = 7-10 per group), and thermogenesis (n = 5-7 per group). Histological and apoptosis analyses were conducted in adipose-associated ganglia and sympathetic nerve fibres from high-fat diet-fed obese mice (n = 5 per group). Human genetic association analyses were performed in a European cohort (n = 346,177 individuals) from the UK Biobank.

Data are presented as mean ± SEM. Statistical analyses were performed using unpaired two-tailed Student's t-tests or one- or two-way ANOVA with appropriate post hoc corrections, as applicable. Statistical significance was defined as $p < 0.05$.

All animal procedures were conducted in accordance with the UK Animals (Scientific Procedures) Act 1986 and approved by the institutional Animal Welfare and Ethical Review Body. Human genetic analyses were performed on de-identified data from approved cohorts with relevant ethics committee approval.

Results:

Using single-cell RNA sequencing on murine sympathetic ganglia, we identified a unique population of perineurial cells expressing both the leptin receptor (*Lepr*) and the β2 adrenergic receptor (*Adrb2*)[4]. **S**ympathetic **P**erineurial **C**ells (SPCs) form a barrier surrounding sympathetic ganglia and nerve bundles in adipose tissue and display molecular features resembling endothelial cells. Conditional knockout of Adrb2 in *Lepr*$^+$ SPCs predisposes mice to obesity by lowering energy expenditure and thermogenic activity without affecting food intake. Notably, we found that obesity-driven hyperleptinemia causes apoptosis in SPCs, leading to a significant erosion of the perineurial barrier and concomitant sympathetic neuropathy. We further show that this deleterious effect can be reversed by partial reduction of leptin or by β2 adrenergic receptor agonism. Supporting translational relevance, we confirmed the presence of *LEPR*$^+$ *ADRB2*$^+$ SPCs in human sympathetic ganglia. We also observed a synergistic effect of highly common polymorphisms in *LEPR* and *ADRB2* on the risk of increased BMI in a large European population.

Conclusion:

These findings identify SPCs as a critical neuroendocrine interface integrating leptin and sympathetic signalling in adipose tissue and support a revised model of the leptin set point beyond central appetite regulation.

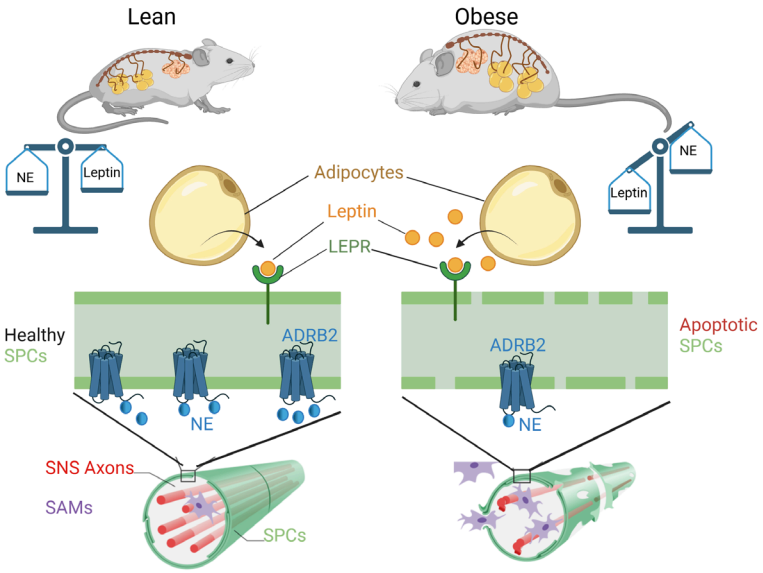

Graphical illustration. The *Lepr*$^{+}$ *Adrb2*$^{+}$ SPCs can sense and integrate leptin and norepinephrine (NE) signalling in adipose tissue that form the afferent and efferent arms of the neuroendocrine loop of leptin action, respectively. In obesity, when leptin signalling exceeds the norepinephrine released by sympathetic nerves, SPCs undergo apoptosis, which erodes the neuroprotective perineurial barrier, exposing sympathetic neurons to pro-inflammatory cues. Altogether, this contributes to sympathetic neuropathy and disrupts adipose tissue homeostasis. Created with BioRender.com.

C07

Betaine ameliorates doxorubicin-induced cardiorenal toxicity in rats.

Mateusz Koper[1], Izabella Mogilnicka[1], Kinga Jaworska[1], Wojciech Kopacz[1], Mateusz Szudzik[1], Emilia Samborowska[2], Marcin Ufnal[1]

[1]Department of Experimental Physiology and Pathophysiology, Laboratory of the Centre for Preclinical Research, Medical University of Warsaw, Warsaw, Poland, [2]Mass Spectrometry Laboratory, Institute of Biochemistry and Biophysics, Polish Academy of Sciences, Warsaw, Poland

Introduction: Doxorubicin (DOX) is a potent chemotherapeutic agent whose clinical utility is severely limited by dose-dependent cardio- and nephrotoxicity. Betaine, a methyl donor and major renal osmolyte, has been suggested to maintain cardiovascular homeostasis and improve renal function through antioxidant and potential diuretic mechanisms[1, 2].

Aims: This study evaluated the protective effects of betaine against DOX-induced injury in heart and kidney tissues by assessing hemodynamic, biochemical, and molecular parameters.

Methods: Male Sprague-Dawley rats (n=36) were randomized into four groups: Control (tap water; n= 8); Betaine (0.5% solution in water, n= 8); DOX (i.p. injections, cumulative dose 15 mg/kg bw, n=10); and DOX+Betaine (n=10). After eight weeks, 24-hour water and food balance were evaluated in metabolic cages. Subsequently, echocardiography and hemodynamic recordings were performed under urethane anaesthesia (1.5 g/kg bw i.p.). Plasma NT-proBNP and urinary KIM-1 were measured via ELISA. Biochemical parameters including proteinuria were determined using a Cobas 6000 analyzer. Antioxidant enzymes (catalase, SOD1) were quantified by Western blot in the heart, renal cortex, and medulla. Data were analyzed via ANOVA with Tukey's or Kruskal-Wallis with Dunn's post-hoc tests ($p < 0.05$). All procedures were approved by the Local Ethics Committee and accorded with international guidelines and legislation.

Results: DOX administration significantly increased mean arterial blood pressure (MABP) (DOX: 134.6±2.6 vs Control: 115.3±2.3 mmHg; $p < 0.001$) and plasma NT-proBNP levels (51.8±5.1 vs 22.8±3.7 pg/ml; $p = 0.009$). Renal damage was evidenced by elevated urinary KIM-1 (6352±279 vs 2781±597 pg/ml; $p < 0.001$) and marked proteinuria (2018.9±1320 vs 144.9±41.3 mg/dl, $p < 0.001$). Histopathological analysis confirmed morphological damage in both cardiac and renal tissues. Betaine supplementation significantly attenuated proteinuria (639.7±439.6 mg/dl, $p < 0.05$ vs DOX) and urinary KIM-1 levels (2376±342 pg/ml, $p < 0.05$ vs DOX). It also partially mitigated the rise in MABP (125.9±3.5 mmHg) and NT-proBNP (38.3±7.7 pg/ml), while improving tissue morphology. Notably, betaine did not significantly alter urine excretion rates or the expression of antioxidant enzymes (SOD1, catalase) in the heart or kidney. Data are expressed in means±SE.

Conclusions: Dietary betaine provides significant protection against DOX-induced cardiorenal injury. These protective effects appear to be independent of antioxidant enzyme modulation or diuretic actions, suggesting alternative mechanisms of action. These findings support the investigation of betaine as a non-pharmacological dietary strategy to mitigate chemotherapy-induced toxicity.

Figure 1. Box plots showing biochemical markers of kidney damage in experimental groups. * $p < 0.05$ by ANOVA with Tukey's post-hoc test or by Kruskal-Wallis with Dunn's post-hoc test.

Figure 2. Box plots showing NT pro-BNP and hemodynamic parameters in experimental groups. * $p < 0.05$ by ANOVA with Tukey's post-hoc test or by Kruskal-Wallis with Dunn's post-hoc test.

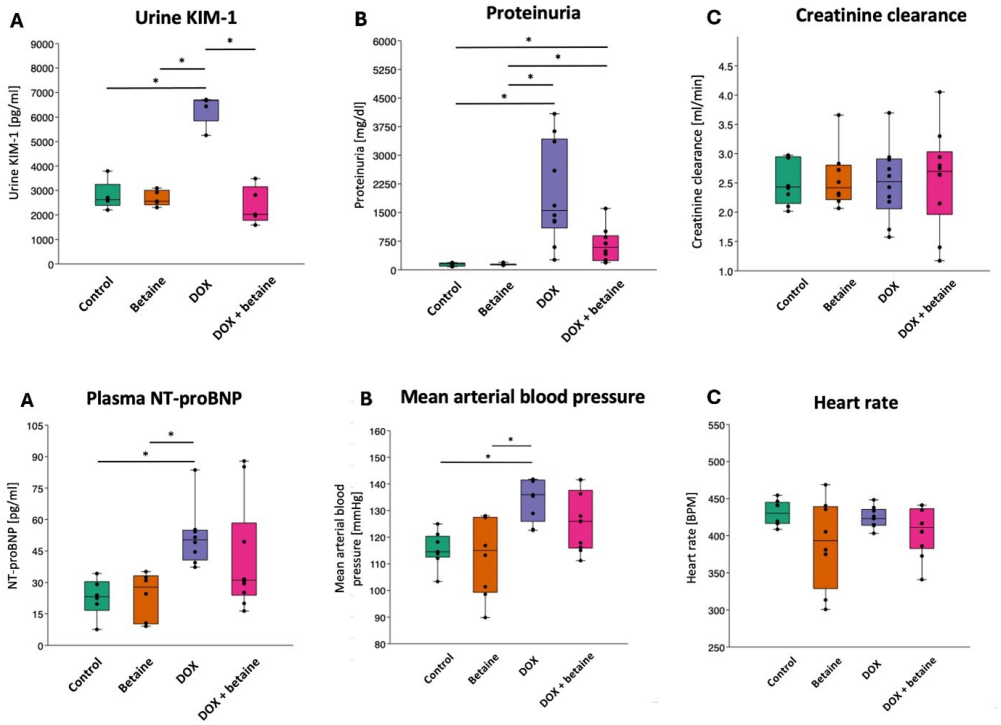

C08

Investigating the effect of oxytocin on the inner and outer layers of the pregnant and non-pregnant human myometrium

Poppy F White[1], Chris J Hill[2], Lorna Salvini[2], Dharani K Hapangama[2], Sarah Arrowsmith[1]

[1]Manchester Metropolitan University, United Kingdom, [2]University of Liverpool, United Kingdom

Introduction:

Contractions of the myometrium, the muscle layer of the uterus, serve several physiological functions including menstruation and labour, with aberrant contractions associated with benign gynaecological disorders and obstetric complications such as adenomyosis and dystocia. The myometrium consists of three layers: the sub-endometrial inner (IM), sub-serosal outer (OM), and middle myometrium. Despite animal studies suggesting distinct contractile properties and physiological functions of the IM and OM, equivalent functional characterisation in humans is lacking.

Aim:

To characterise regional differences in the effect of oxytocin on human myometrium.

Methods:

Myometrial biopsies were collected from term-pregnant women undergoing elective caesarean section (n=17) and nonpregnant women (n=4) undergoing hysterectomy for benign gynaecological conditions at Liverpool Women's Hospital with informed, written consent and REC approval (REC 10/H1002/49).

Paired strips (5x2x1mm) from the IM and OM were mounted in organ baths to record isometric tension. The effect of oxytocin (10^{-10}-10^{-6}M) on contraction amplitude (mN), mean integral of force (MIF, a.u), frequency (contractions/hour), and duration (min) were assessed relative to spontaneous contractions (taken as 100%). Concentration-response curves determined maximum effect (Emax). OM and IM responses were compared via paired Student's t-test or Wilcoxon signed rank test, $P<0.05$ was significant.

Results:

Mean amplitude of pregnant IM spontaneous contraction was greater (9.27mN, SE 1.61) than the OM (6.24mN, SE 0.91) but not significant ($P=.06$, n=17). Similarly, nonpregnant IM mean contraction amplitude was greater (6.12mN, SE 2.18) than the OM (3.94mN, SE 0.807) ($P=.31$, n=4). No significant regional differences in duration, frequency, or MIF of spontaneous contractions were observed in the pregnant or nonpregnant myometrium.

Oxytocin increased mean contraction amplitude and MIF in both regions of the pregnant myometrium in a concentration-dependent manner (n=10). Amplitude Emax in the OM was 256% of control (SE 39.6) compared to 163% (SE 15.4) in the IM, but not significantly greater (*P*=.06). Overall MIF Emax in the OM and IM was equal; OM, 322% of control (SE 51.0) and IM, 328% of control (SE 45.2) (*P*=.1). A dose-dependent reduction in contraction frequency and prolongation of duration was observed in both layers, with no regional difference noted.

Similarly, a dose-dependent stimulatory effect of oxytocin on contraction amplitude and MIF was demonstrated in both regions of the nonpregnant myometrium (n=4). Contrasting with the pregnant myometrium, a trend toward increased response in the IM compared to the OM was observed. Dose-response curves were not fit due to sample size.

Comparing oxytocin's effect in the pregnant and nonpregnant myometrium, oxytocin induced a significantly smaller uterotonic effect in the nonpregnant OM compared to the pregnant OM; 114% of control (SE 7.20) vs. 233% (SE 40.1) (*P*=.04). The same trend was observed in the IM, although not significant.

Conclusions:

Regional specific differences in spontaneous myometrial contractile activity highlight potential functional differences between the IM and OM, possibly supporting distinct physiological roles. An increased response to oxytocin in the pregnant myometrium and specifically in the OM, supports the proposed role of the OM in facilitating the powerful contractions in labour. The opposite layer-specific sensitivity to oxytocin in the nonpregnant myometrium may indicate processes relevant to nonpregnant uterine function, which warrant further investigation.

C09

The Role of Transient Receptor Potential Vanilloid 4 (TRPV4) in Regulating Murine Hair Growth and Follicle Density

Ammar Boudaka[1], Mallak AlYazeedi[2], Intisar Al Lawati[3]

[1]Department of Basic Medical Sciences, College of Medicine, QU Health, Qatar University, Qatar, [2]Sultan Qaboos University, College of Medicine and Health Sciences, Oman, [3]College of Medicine and Health Sciences, Oman

Title: The Role of Transient Receptor Potential Vanilloid 4 (TRPV4) in Regulating Murine Hair Growth and Follicle Density

Introduction: Hair growth is a highly regulated physiological process characterized by cyclical phases of active growth (anagen), regression (catagen), and rest (telogen). Fundamental to this morphogenesis is calcium signaling, which modulates the release of essential growth factors such as TGF-alpha and EGFR. While other members of the transient receptor potential (TRP) family, such as TRPV1 and TRPV3, have established roles in hair cycle regulation, the specific contribution of the calcium-permeable cation channel TRPV4—expressed widely in skin keratinocytes—remains largely uncharacterized.

Aims/Objectives: The primary objective of this study was to investigate the physiological impact of TRPV4 deletion on hair regrowth in a murine model. Specific aims included: 1) Evaluating the progression of hair regrowth via digital analysis; 2) Quantifying growth parameters, including hair length ratio and weekly growth rates; and 3) Conducting histological assessments to compare hair follicle density between wild-type (WT) and TRPV4 knockout (TRPV4KO) mice.

Methods: All experimental procedures were conducted in accordance with institutional ethical standards for animal care at Qatar University and Sultan Qaboos University. Male C57BL/6NCr (WT) and TRPV4KO mice (9–11 weeks old; n=4 per group based on representative visual data) were used. Under anesthesia, the back and abdominal regions were shaved and treated with hair removal cream. Hair regrowth was monitored weekly for four weeks through digital photography. Three hairs were collected per week from each region to calculate the average length, length ratio, and growth rate. At week 4, skin biopsies were obtained, stained with Hematoxylin and Eosin (H&E), and scanned to quantify hair follicle density within a 1.2 cm area. Statistical analysis was performed using t-tests, with data presented as mean ± SEM.

Results: Visual assessment confirmed that hair regrowth was markedly delayed in TRPV4KO mice compared to WT. In the **back region**, TRPV4KO mice exhibited a significantly lower hair length ratio at week 1 ($p < 0.05$) and week 2 ($p < 0.001$). Similarly, the back hair growth rate was significantly reduced in KO mice during week 1 ($p < 0.05$) and week 2 ($p < 0.001$). Histological analysis at week 4 revealed that TRPV4KO mice had significantly fewer hair follicles in the back region compared to WT ($p < 0.05$). Conversely, the **abdominal region** showed more resilience, with significant decreases in growth rate appearing only by week 4 ($p < 0.05$), while the hair length ratio showed no significant difference throughout the study.

Conclusions: These findings demonstrate that **TRPV4 is a positive regulator of hair growth in mice**. Its deletion results in a significant delay in the hair growth cycle and a reduction in follicle density, likely due to impaired calcium signaling affecting the proliferation of matrix cells. The regional variations observed suggest that TRPV4 influence may depend on the specific physiological environment of the follicles.

Consequently, TRPV4 represents a potential therapeutic target for the management of hair loss and growth disorders.

C10

The Prognostic Value of Skin Temperature Variability Analysis in Humans: A Systematic Review

Eubi Chan[1], Angelica Blotto[1], Ali R. Mani[1]

[1]Network Physiology Laboratory, UCL Division of Medicine, London, UK, United Kingdom

Introduction:
Skin temperature fluctuates dynamically and reflects complex thermoregulatory mechanisms, including the balance between heat loss and heat gain mechanisms through autonomic control of peripheral blood flow and metabolic factors. While analytical methods have been established to assess skin temperature variability (STV), the potential applications of STV analysis remain an emerging and primarily exploratory field. This systematic review aims to synthesize current evidence on the prognostic role of STV metrics, including short-term fluctuations, circadian patterns, and entropy in predicting clinical outcomes such as mortality. It also seeks to characterise the technical heterogeneity in measurement sites and analytical approaches, and to identify future research directions.

Methods:
Following PRISMA guidelines, a systematic search was conducted across Ovid MEDLINE, EMBASE, and AMED from inception to July 2025. Studies were eligible if they included human participants in any clinical setting and linked dynamic STV measurements to prognostic outcomes. The quality of the included studies was assessed using the QualSyst tool. As this study is a systematic review of previously published data and did not involve new data collection from human participants or animals, no ethical approval was required.

Results:
Of 123 papers screened, a total of 8 studies met the inclusion criteria. Preliminary evidence suggests an association between altered STV and patient prognosis, although the findings are limited by methodological heterogeneity:

1. **Population-Level Findings:** Large-scale data from the UK Biobank (n=91,462) identified that blunted circadian temperature amplitudes are independent predictors of long-term incident diseases, including Non-alcoholic Fatty Liver Disease (HR: 1.91) and Type 2 Diabetes (HR: 1.69).

2. **Clinical Cohort Findings:** Seven smaller observational cohorts (n=21 to 66) demonstrated that reduced signal complexity (entropy), loss of short-term variability, and increased thermal instability were associated with higher mortality risks (OR: 1.41) and lower event-free survival across acute and chronic conditions, including sepsis, cirrhosis, and ischaemic heart disease.

3. Methodological Heterogeneity: Significant variability was observed across studies regarding measurement sites (e.g., axilla, wrist, hypochondrium), sampling frequencies (ranging from every 10 seconds to three times daily), and analytical approaches, including amplitude, entropy, and short- and long-term variability.

A process-based logic model was developed to map the conceptual relationships between patient populations, measurement sites, STV metrics, and clinical outcomes (Figure 1).

Conclusion:
STV analysis shows promise as a non-invasive tool for identifying physiological vulnerability across a wide spectrum of clinical conditions. However, the current evidence is predominantly exploratory and constrained by small sample sizes and high methodological heterogeneity. Future research should focus on large-scale validation studies and standardizing STV metrics to facilitate their integration into wearable technology and real-time clinical monitoring systems.

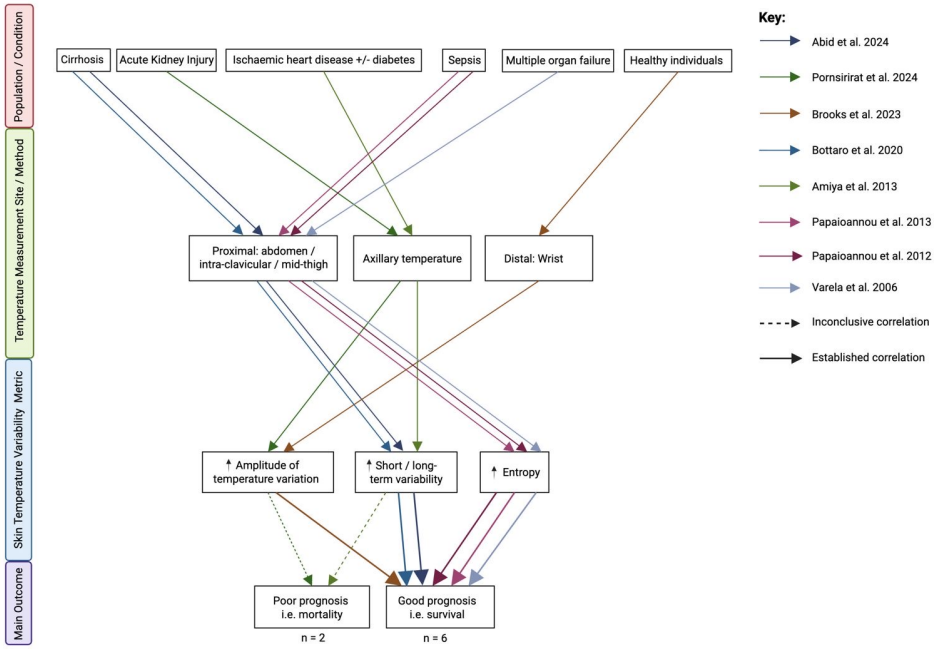

Figure 1. Process-based logic model of relationships between population/condition, temperature measurement site/method, skin temperature metric, and clinical outcomes across included studies. Key: coloured arrows represent individual studies (see author/year labels), dashed arrows indicate inconclusive correlations, and thicker solid arrows indicate established correlations. Arrow direction shows the relationship between variables. 'n' denotes the number of studies contributing to each prognosis category.

C11

Non-invasive assessment of autonomic and endothelial functions in patients with migraine and healthy individuals.

Sadia Anjum [1], Dr. Shobitha muthukrishnan [2], Dr. Anita S Malhotra [3]

[1]Sharda school of medical sciences and research, sharda university, india, [2]Sharda school of medical sciences and research, sharda university, India, [3]Govt. medical; college and hospital, Chandigarh, INDIA

Introduction

Migraine is a complex neurovascular disorder whose triggers are not entirely understood. Autonomic and endothelial dysfunction might play a role in migraine. Migraine headache (MH) is associated with nausea, vomiting, and uneasiness in the presence of light and sound. It is characterised by multiple episodes of throbbing pain originating in one side of the head.

Aim

This study aims to describe the cardiovascular, autonomic and endothelial functions in patients with migraine and healthy controls.

Material and methods

This study evaluated the cardiovascular autonomic function and endothelial function tests. The study was done on 85 healthy volunteers within the age group of 18 to 55 as a control group and 85 patients with migraines as the study group. The standard autonomic cardiovascular function tests, such as heart rate variability for autonomic tone & for autonomic functions reactivity and standard cardiovascular Ewing tests[14] for both parasympathetic and sympathetic divisions, were performed. Non-invasive assessment of endothelial function was performed by brachial artery flow-mediated dilation (FMD). FMD reflects endothelial-dependent vasodilation mediated mainly by Nitric oxide (NO)

Results

In this study, we found that females were affected more than males. We observed reduced parasympathetic activity in patients with migraine as compared to healthy controls. Flow-mediated dilatation (FMD) is a well-established, non-invasive marker of endothelium-dependent vasodilation, primarily mediated by nitric oxide (NO) release. The significantly reduced FMD percentage observed in migraine patients indicates endothelial dysfunction, despite comparable baseline brachial artery diameters

Discussion

The ANS is strongly influenced by sympathetic and parasympathetic divisions. Flow-mediated dilation (FMD) was significantly reduced in patients with migraine, indicating the presence of endothelial dysfunction. Reduced FMD can be linked to increased cardiovascular risks in patients with migraine.

C12

Effects of HO-1/CO on Oxidative Stress and Inflammation in Human Bronchial Epithelia

Wing Hung KO[1], Chung Yin YIP[1], Chiamaka AMARACHUKWU

[1]The Chinese University of Hong Kong, Hong Kong

Oxidative stress and chronic inflammation are key elements of human airway and lung diseases. Harmful gases, such as cigarette smoke or noxious particles, stimulate neutrophils and macrophages to produce inflammatory cytokines and mediators, leading to inflammation and a subsequent increase in reactive oxygen species (ROS). As a result, oxidative stress escalates, promoting a broad spectrum of immune disorders and pathophysiological conditions, including chronic obstructive pulmonary disease (COPD). Heme oxygenase (HO), a family of enzymes that manage the cellular response to oxidative stress, is known to degrade heme (the precursor to hemoglobin) to reduce oxidative stress, restore intracellular redox balance, and maintain cellular homeostasis. HO enzymes, particularly the inducible isozyme HO-1, produce carbon monoxide (CO), biliverdin, and iron in mammalian cells. HO-1 activity is upregulated by cellular stress in all tissues, including the brain. However, the precise mechanisms by which HO-1 exerts these anti-inflammatory and anti-oxidative effects in human bronchial epithelia remain unclear. The purpose of this study is to investigate how HO-1/CO modulates oxidative stress and inflammation in human bronchial epithelium.

In this study, we used three different human bronchial epithelial (16HBE14o-) cell models: wildtype (WT), H25A (HO-1 inactive) mutant, and HO-1 knockdown (KD). Intracellular ROS was measured using the cell-permeable probe, 2',7'-dichlorodihydrofluorescein diacetate (H2DCFDA), by fluorescence microscopy. A cytokine array analysis was used to detect the expression levels of 80 human cytokines semi-quantitatively. The data show that ROS fluorescent intensity increased significantly in KD ($p < 0.01$) and H25A mutant cells ($p < 0.001$) after stimulation with hemin, a well-known oxidative inducer ($n = 4$; one-way ANOVA followed by Tukey's multiple comparison test). Therefore, in the presence of a previous oxidative factor or stimulus, a decrease in HO-1 expression or mutation of HO-1 resulted in greater levels of ROS, indicating high oxidative stress. Cytokine array analysis data show that in HO-1 KD cells, pro-inflammatory mediators MCP-1 (CCL2), IL-8, IL-6, TIMP-1 and BDNF were increased , while anti-inflammatory mediators IGFBP-3 and RANTES (CCL5) were decreased ($n = 3$). In H25A mutant cells, pro-inflammatory cytokines TNF-α, IL-8, and IL-6 were reduced ($n = 3$). Our findings suggest that HO-1 regulates cellular oxidative stress and exerts an anti-inflammatory effect in human bronchial epithelial cells. These findings offer insight into some of the mechanisms that underpin HO-1 activity as a therapeutic strategy for oxidative stress-related respiratory diseases.

C13

Betaine improves cardiac function and reduces myocardial fibrosis in aged hypertensive rats.

Wojciech Kopacz[1], Kinga Jaworska[1], Mateusz Koper[1], Magdalena Rybaczewska[1], Monika Kuś[1], Emilia Samborowska[2], Marcin Ufnal[1]

[1]Department of Experimental Physiology and Pathophysiology, Laboratory of the Centre for Preclinical Research, Medical University of Warsaw, Warsaw, Poland, Poland, [2]Mass Spectrometry Laboratory, Institute of Biochemistry and Biophysics, Polish Academy of Sciences, Warsaw, Poland, Poland

Introduction: Hypertension induces progressive cardiac remodeling, including myocardial fibrosis and impaired ventricular function [1]. Increasing evidence suggests that organ protection independent of blood pressure reduction is clinically relevant. Betaine, a naturally occurring osmolyte, is depleted in hypertensive states and may contribute to organ vulnerability [2, 3]. However, the long-term effects of betaine supplementation on cardiac structure and function remain unclear.

Aim: This study aimed to determine whether chronic betaine supplementation improves cardiac function and attenuates markers of organ damage in aged spontaneously hypertensive rats (SHR).

Methods: Male SHR (n=20) were treated from 8 to 78 weeks of age with either tap water (control) or betaine supplementation (500 mg/l in drinking water, a dose of approximately 78 ± 15 mg/kg per day. Due to attrition unrelated to the current study, number of animals included in the final analysis were n=8 (control) and n=9 (betaine). Metabolic cage studies assessed 24-hour water and electrolyte balance. Echocardiography was performed. Arterial blood pressure (BP) and heart rate were recorded under urethane anaesthesia (1.5 g/kg, i.p.). Blood and urine samples were collected for biochemical analyses. Post-euthanasia, cardiac and renal tissues were harvested for histopathological and molecular evaluation. Tissue expression of renin-angiotensin system (RAS) components was analyzed via RT-qPCR, and plasma/urine choline metabolites were measured using UPLC. Data were analyzed using Student's t-test or Mann-Whitney U test ($p<0.05$). All procedures complied with Directive 2010/63/EU and were approved by the local ethics committee.

Results: Betaine supplementation significantly increased 24-hour urine output (42.4±18.7 vs 33.3±6.9 mL, $p=0.02$) without affecting plasma or urinary electrolyte levels. Echocardiography revealed improved cardiac function, with higher ejection fraction in betaine-treated rats (69.0±13.01% vs 56.13±12.15%, $p=0.048$). Histopathological analysis demonstrated reduced signs of heart and kidney injury after betaine treatment (Figure 1). Above all, morphometric analysis revealed decreased myocardial fibrosis ($p=0.014$). Molecular analysis revealed minor alterations in RAS components, with increased cardiac AT1A receptor expression ($p=0.047$) and reduced renin expression in the renal medulla ($p=0.05$). Notably, betaine increased circulating choline-derived metabolites, including trimethylamine N-oxide (TMAO) and trimethylamine (TMA)(Table 1).

Conclusions: Chronic betaine supplementation improves cardiac function and reduces myocardial fibrosis, indicating a BP-independent cardioprotective effect. These effects may relate to increased diuresis and attenuation of pathological remodeling. These benefits may be linked to increased diuresis and the attenuation of pathological remodeling. However, the concomitant increase in potentially pro-atherogenic choline-derived metabolites suggests a complex metabolic profile that warrants further investigation.

Figure 1. Histopathological findings in Spontaneously Hypertensive Rats on water (SHR-Water) or betaine (SHR-Betaine). Values are means±SE, p values by t-test or U Mann Whitney, depending on the normality of the data distribution.

Table 1. Plasma and urinary concentrations of choline-derived metabolites, including trimethylamine N-oxide (TMAO), trimethylamine (TMA), betaine, glycerophosphocholine (GPC), and carnitine, in experimental groups.

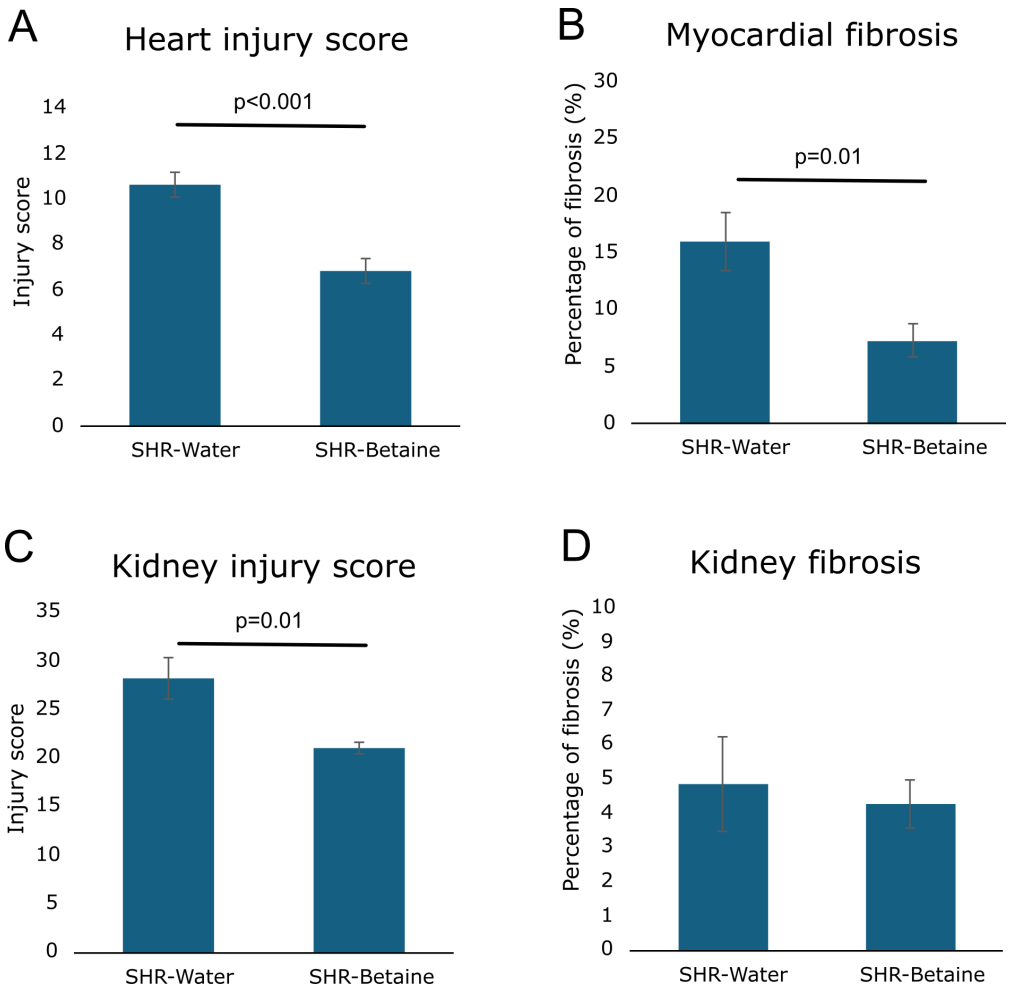

Parameter	Control SHR	Betaine SHR	p
PLASMA			
TMAO (µmol/L)	2.09 ± 0.62	141.51 ± 122.49	**0.0385**
TMA (µmol/L)	0.00 ± 0.00	0.51 ± 0.37	**0.0039**
Betaine (µmol/L)	91.30 ± 43.62	77.56 ± 14.23	0.4939
GPC (µmol/L)	133.83 ± 95.58	78.70 ± 54.63	0.2551
Carnitine (µmol/L)	25.71 ± 4.98	19.03 ± 4.13	**0.0306**
URINE			
TMAO (µmol/L)	321.03 ± 112.19	6698.13±1834.83	**0.0004**
TMA (µmol/L)	3.23 ± 1.54	30.13 ± 10.75	**0.0046**
Betaine (µmol/L)	258.41 ± 56.03	22494.09±8337.42	**0.0013**
GPC (µmol/L)	20.99 ± 7.80	14.48 ± 10.89	0.2643
Carnitine (µmol/L)	26.06 ± 11.24	32.22 ± 7.08	0.2403

Table 1. Plasma and urinary concentrations of choline-derived metabolites, including trimethylamine N-oxide (TMAO), trimethylamine (TMA), betaine, glycerophosphocholine (GPC), and carnitine, in experimental groups.

C14

Oral P2X3 antagonism reduces carotid chemoreflex sensitivity in healthy adults.

Florence Mouy[1], Hazel Blythe[1], Lydia Simpson[1], Tim Swinn[1], Julian FR Paton[2], Angus K Nightingale[3], Emma C Hart[1]

[1]University of Bristol, United Kingdom, [2]University of Auckland, New Zealand, [3]University Hospitals Bristol and Weston NHS Foundation Trust, United Kingdom

Introduction

The carotid body has a key role in the control of breathing in humans[1]. There is now strong evidence that the carotid chemoreflex, is overactive in a range of conditions such as heart failure[2] and COPD[3]. Dopamine has been used to inhibit the carotid chemoreflex but its use is limited by its intravenous access[4], short half-life and non-selective nature. Our group has shown that P2X3 receptors in the carotid body can be targeted to reduce carotid chemoreflex overactivity in animal models of hypertension[5] and heart failure[6]. Whether P2X3 receptor antagonism in humans impacts carotid chemoreflex control of ventilation is unknown.

Objective

Our objective was to assess whether oral P2X3 antagonism with gefapixant influences the carotid body chemoreflex and breathing during exercise, in healthy adults.

Hypothesis

We hypothesised that oral P2X3 antagonism would reduce carotid chemoreflex sensitivity and temper ventilation during exercise in healthy adults.

Methods

This was a pilot feasibility crossover study. Healthy adults with no major co-morbidities were recruited. Participants received an acute oral dose of gefapixant (45 mg) and placebo (randomised in order and double-blinded). Participants underwent testing for the hypoxic ventilatory response (HVR; via intermittent hypoxia induced by added nitrogen), a measure of carotid chemoreflex sensitivity, as well as cardiopulmonary exercise testing (CPET), to assess ventilatory responses to exercise (ramped incremental exercise test on cycle ergometer; Lovemedical Ergostik CPET system). HVR was evaluated as the slope of the linear regression relating the minute ventilation (VE) to the nadir of oxygen saturation for each nitrogen exposure. Data were compared with a Wilcoxen matched pairs test. Data are median with range.

Results

Four participants (3 males, age; 47 [IQR 39-52] years and BMI; 23 [IQR 21-25] kg/m^2) volunteered to participate (REC number 25/HRA/0973). Gefapixant reduced the HVR compared with placebo (-0.24 [-0.30 to -0.14] L/min/% vs -0.31 [-0.34 to -0.21] L/min/%; p=0.0209, effect size Cohen's dRM=3.5). The VE/volume of CO2 expired (VE/VCO2) nadir during CPET was also decreased by gefapixant (23.7±1.9) vs. placebo (24.8±1.5), p=0.0531, effect size Cohen's dRM= -2.19. Importantly, no side effects or adverse events were reported. Gefapixant did not impact maximum heart rate, peak oxygen consumption (VO2)

or exercise duration, compared with placebo (171bpm vs 173bpm, p=0.8088; 41.5ml/min/kg vs 43.3ml/min/kg, p=0.2530; 837s vs 868ms, p=0.3646, respectively).

Conclusion

This is the first study in humans to demonstrate that oral P2X3 antagonism with gefapixant reduces carotid chemoreflex sensitivity to hypoxia. We also found that gefapixant may improve ventilatory efficiency (VE/VCO2 nadir) during exercise. Future studies are required to assess the potential physiological effects in patients with exaggerated carotid chemoreflex functions such as heart failure.

C15

Divergent Hemodynamic Responses to Trimethylamine (TMA) in Hypertensive Rats: Uncovering a Novel Role for the TAAR5 Receptor

Kinga Jaworska[1], Magdalena Rybaczewska[1], Monika Kuś[1], Marcin Ufnal[1]

[1]Department of Experimental Physiology and Pathophysiology, Laboratory of the Centre for Preclinical Research, Medical University of Warsaw, Warsaw, Poland

ABSTRACT

Introduction: We have previously demonstrated that the gut microbiome metabolite trimethylamine (TMA) exerts significant hemodynamic effects, notably a pronounced hypertensive response [1]. While the Trace Amine-Associated Receptor 5 (TAAR5) is a known molecular target for TMA, its physiological role has been studied almost exclusively within the central nervous system [2], with its peripheral cardiovascular functions remaining unexplored. Furthermore, it remains unknown whether TMA-induced cardiovascular responses differ in the setting of established hypertension.

Aims: To investigate the dose- and strain-dependent hemodynamic responses to intravenous TMA in normotensive Wistar-Kyoto (WKY) and Spontaneously Hypertensive Rats (SHR), and to determine if these cardiovascular effects are mediated by the TAAR5 receptor.

Methods: WKY and SHR rats (n=5-6 per strain and dose) received intravenous TMA at doses of 45, 135, and 405 µmol/kg. Blood pressure (BP) was continuously monitored for 20 minutes under urethane 1.5 g/kg i.p. anaesthesia. To assess the mechanistic role of TAAR5, a subset of WKY rats was pretreated with a TAAR5 inhibitor (Z1230215228, Enamine, equimolar dose, i.v.) prior to the 135 µmol/kg TMA challenge. Baseline TAAR5 mRNA expression was quantified via RT-qPCR in the heart (right and left ventricle), kidney (medulla and cortex), jejunum, colon, and liver of both strains. All procedures accorded with Directive 2010/63/EU and were approved by Local Bioethical Committee.

Results: At the lowest TMA dose (45 µmol/kg), rats exhibited a distinctly strain-dependent hemodynamic response (Two-way mixed ANOVA, Time × Strain interaction, $p<0.001$, Figure 1A,B). While both strains displayed a biphasic BP reaction, the subsequent hypertensive rise was significantly less pronounced in SHR compared to WKY (BP WKY vs SHR $p<0.05$ from minute 13 through minute 20 post-injection, independent t-tests, Holm-Bonferroni corrected). Concurrently, TMA induced a significant drop in HR in SHR at both 45 and 405 µmol/kg doses, whereas HR in WKY rats remained unchanged (Two-way mixed ANOVA, Time × Strain interaction, $p<0.001$). At higher doses (135 and 405 µmol/kg), the temporal BP trajectories did not significantly differ between strains. Mechanistically, pretreatment with the TAAR5 inhibitor in WKY rats significantly attenuated the TMA-induced hypertensive response (Peak MABP within the first 10 min: 7.50±0.88 vs. 14.78±2.64 mmHg, $p=0.03$, Welch's t-test, Figure 1C). Tissue profiling revealed ubiquitous TAAR5 expression across all studied organs; notably, baseline TAAR5 expression was significantly upregulated in the left ventricle and colon of SHR compared to WKY rats. (Figure 2).

Conclusion: TMA elicits a dose-dependent, biphasic hemodynamic response, with the pressor phase being significantly blunted in hypertensive subjects, likely driven by a strain-specific bradycardic reflex. In normotensive rats, this TMA-induced pressor effect is mediated by the TAAR5 receptor, providing the first direct evidence of its peripheral cardiovascular function. Furthermore, the targeted upregulation of TAAR5 in the left ventricle and colon of SHR offers a plausible molecular basis for their altered reflex, pointing toward a disease-specific remodeling of the microbiome-cardiovascular axis in hypertension.

However, further functional studies in hypertensive models are warranted to confirm this direct mechanistic link.